Reduced ferromagnetic transition temperatures in $SrRu_{1-v}O_3$ perovskites from Ru-site vacancies

B. Dabrowski, O. Chmaissem, P. W. Klamut, S. Kolesnik, M. Maxwell, J. Mais, Y. Ito, and B. D. Armstrong
Department of Physics, Northern Illinois University, DeKalb, Illinois 60115, USA

J. D. Jorgensen and S. Short
Materials Science Division, Argonne National Laboratory, Argonne, Illinois 60439, USA
(Received 26 January 2004; published 21 July 2004)

We show that annealing of stoichiometric $SrRuO_3$ perovskites in high-pressure oxygen of 600 atm near 1100 °C produces $SrRu_{1-v}O_3$ compounds with vacancies on the Ru-sites. The creation of Ru vacancies rapidly suppresses the ferromagnetic ordering temperature, T_C, from 163 K to 45 K with an increase of $v \approx 0.09$. Subtle structural changes that accompany the creation of Ru-site vacancies are different from the typical properties of transition metal perovskites, for which an increased formal oxidation state of the B-site cations normally leads to decreased B-O interatomic distances and contraction of the unit cell volume. The reduced charge screening caused by the Ru-vacancies offsets an expected decrease of the average interatomic distance Ru-O and rotation of the RuO_6 octahedra as Sr atoms relax toward Ru-vacancies increases the observed volume.

DOI: 10.1103/PhysRevB.70.014423 PACS number(s): 61.66.Fn, 61.12.−q, 75.90.+w

I. INTRODUCTION

$SrRuO_3$ is known as a highly correlated, narrow-band metallic ferromagnet with a robust Curie temperature $T_C \approx 160$ K.[1] Ferromagnetism in $SrRuO_3$ arises from a parallel alignment of the low-spin electronic configuration of Ru^{4+} t_g^4 electrons. The low-temperature ordered magnetic moment of $SrRuO_3$ showing a lack of saturation to the full $S=1$ moment ($2\mu_B$/Ru atom) in dc fields to 30 T when considered together with the good metallic conductivity is consistent with itinerant ferromagnetism.[2] Greater overlap and hybridization between the 4*d* orbitals of Ru and O 2*p* orbitals are expected to lead to greater itinerancy and more interplay between structural degrees of freedom and magnetic and electronic properties. Recent first principles studies by Mazin and Singh (Ref. 1) have shown that oxygen *p*-derived states participate substantially in the magnetism and the electronic structure near the Fermi energy. These authors have also shown that differences in the magnetic ground states of paramagnetic $CaRuO_3$ and $SrRuO_3$ are due to complex band structure effects related to the modulation of the Ru-O hybridization by the increased structural distortion. In addition to unique ferromagnetism among 4*d* perovskites, the $SrRuO_3$ compound has been intensively studied for possible application as an electrode material in microelectronic circuits.[3] More recently, Fang *et al.*[4] have reported the observation of magnetic monopoles in $SrRuO_3$ in the context of the anomalous Hall effect.

Moderately reduced Curie temperatures have been observed for thin films of $SrRuO_3$ deposited on substrates with mismatched lattice parameters and explained in terms of strain effects[5] consistent with the observations of a decrease of T_C with applied hydrostatic pressure in bulk samples.[6] Reduced Curie temperatures were also observed for some single crystals that were grown in alumina crucibles but these suppressed T_C's are most probably caused by unintentional impurity substitutions. Recently, Joy *et al.*[7] suggested that the Curie temperature of $SrRuO_3$ could depend on the synthesis temperature in oxygen. They reported the existence of two different phases, a phase with $T_C=141$ K formed below 1100 °C and the more commonly observed phase with $T_C=160$ K obtained for synthesis at higher temperatures. Both phases have orthorhombic crystal symmetry with a marginal difference of their lattice parameters. The results of several substitution studies,[8–10] have shown that the dominant factor controlling the decrease of T_C is a change of the formal oxidation state of Ru with the highest T_C being observed for Ru^{4+}. For substitutions retaining a formal oxidation state of Ru^{4+}, the T_C decreases as a function of decreasing Ru-O-Ru bond angle (Refs. 1 and 2).

The effects of cation and oxygen nonstoichiometry on the physical and structural properties of transition-metal perovskites were studied most extensively for 3*d* transition metals. In this paper, we report synthesis methods that can be used to create Ru-site vacancies, use neutron powder diffraction to determine the vacancy concentration, and establish the relationship between vacancy concentration and T_C. Synthesis methods in air and argon are used for obtaining single-phase stoichiometric $SrRuO_3$ samples. These samples are then converted to nonstoichiometric $SrRu_{1-v}O_3$ compounds using high-pressure oxygen annealing. Energy dispersive x-ray spectroscopy and neutron powder diffraction measurements on $SrRu_{1-v}O_3$ show that under oxidizing conditions vacancies are created on the Ru crystallographic site, analogous to what also occurs in the $LaMn_{1-v}O_3$ perovskites.[11] Investigation of the structural, magnetic, and resistive properties shows that the ferromagnetic transition temperature is decreased dramatically by the creation of Ru vacancies.

II. SAMPLE PREPARATION AND EXPERIMENTAL DETAILS

Polycrystalline samples of stoichiometric $SrRuO_3$ and several intentionally nonstoichiometric compositions with

Ru/Sr ratios of $x=0.88$, 0.92, 0.95, 0.98, and 1.05 were synthesized from mixtures of $SrCO_3$ and stoichiometric RuO_2 (prefired in air at 600 °C). Mixtures of the powders were pressed into pellets and fired in air and Ar (~20 ppm O_2) at various temperatures up to 1150 °C with several intermediate grindings. Further annealings were performed in flowing oxygen, air, and Ar at temperatures between 950–1150 °C and at high-pressure oxygen using 600 atm (a total pressure of 3000 atm of 20% O_2 in Ar) for ~20 h using a large capacity internally-heated vertical hot isostatic pressure furnace. Using such synthesis and annealing conditions, several dozens of 1–2 g-size batches of $SrRuO_3$ were obtained, and examined by x-ray powder diffraction on a Rigaku D/MAX Diffractometer using Cu K_α radiation. Selected samples were studied with thermogravimetric analysis on a Cahn TG171 thermobalance, electron microscopy with Hitachi S-4700 scanning electron microscope for energy dispersive x-ray spectroscopy (EDXS) and JEOL 2010F transmission electron microscope for electron energy loss spectroscopy (EELS), and magnetic and resistive measurements using a Quantum Design Physical Properties Measurement System-Model 6000. Time-of-flight neutron powder diffraction data were collected at room temperature on the Special Environment Powder Diffractometer (SEPD) (Ref. 12) at the Intense Pulsed Neutron Source (IPNS). High-resolution backscattering data, from 0.5 to 4 Å, were analyzed using the Rietveld method with the General Structure Analysis System code (GSAS).[13]

For the study of intrinsic Ru-nonstoichiometry of $SrRuO_3$ it was of critical importance to understand how various processing methods affect the sample quality and stoichiometry. It was found that significant problems during synthesis resulted from two properties of RuO_2: the hygroscopic properties of RuO_2 powders at ambient conditions (leading to weighing errors) and conspicuous volatility of RuO_2 at elevated temperatures. For the preparation of stoichiometric samples of $SrRuO_3$ and compositions with Ru/Sr ratios of $x \neq 1$, it was essential to use dry RuO_2 powders and carry out calcination of the starting $SrCO_3$ and RuO_2 mixtures for very short periods of time at temperatures as low as possible, i.e., 700–800 °C. Using these precautions it was possible during synthesis in air to preserve the initial sample stoichiometries and obtain single-phase $SrRuO_3$ samples for $x=1$ [see, Fig. 1(a)] and two-phase samples with $SrRuO_3$ and Sr_2RuO_4 for $x=0.88$, 0.92, 0.95, and 0.98.

Using extensive x-ray diffraction and TGA measurements we observed that the incompletely reacted samples containing RuO_2 and a sample with the initial composition $x=1.05$ showed weight losses and a change of the ratio of phase fractions of $SrRuO_3$ and RuO_2 due to volatilization of RuO_2 at temperatures above 700 °C. Similar measurements performed in air or Ar for samples not containing RuO_2 did not reveal any weight loss due to volatilization to at least 1100 °C. However, the TGA measurements, using slow heating rates in pure oxygen, for the single-phase $SrRuO_3$ samples showed a small reproducible weight gain in the temperature range 700–1000 °C followed by a small weight decrease at 1000–1100 °C. Examination of the x-ray diffraction patterns indicated that small amounts of the RuO_2 impurity phase were produced in samples fired in oxygen at

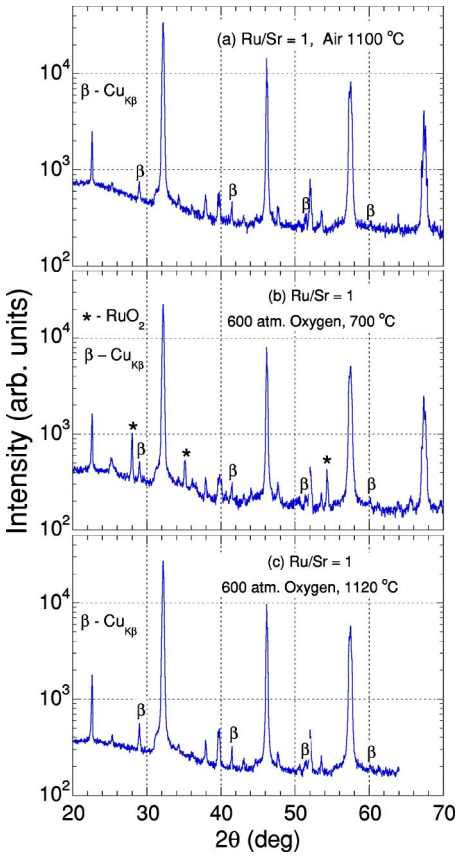

FIG. 1. (Color online) X-ray diffraction patterns for the samples with starting composition $Ru/Sr=x=1$ synthesized in air at 1100 °C (a) and annealed in 600 atm O_2 at 700 °C (b) and 1120 °C (c). The diffraction peaks arising from impurity phase (RuO_2) and incompletely filtered Cu K_β radiation are denoted with asterisk (*) and β, respectively.

~1100 °C. The process of RuO_2 extraction from stoichiometric $SrRuO_3$ compounds in oxygen can be described as an increase of the mass of the solid-state sample according to the chemical reaction $SrRuO_3$ (solid) $+\upsilon O_2 \rightarrow SrRu_{1-\upsilon}O_3$ (solid) $+\upsilon$ RuO_2 (solid), where υ is the amount of Ru vacancies. The RuO_2 solid is then volatilized on prolonged heating leading to an overall decrease of sample mass. This process of formation of Ru vacancies in $SrRu_{1-\upsilon}O_3$ was found to be intrinsic for strongly oxidizing synthesis conditions and could be enhanced by using high-pressure oxygen annealing.

High-pressure oxygen annealing of the stoichiometric $SrRuO_3$ compound and the two-phase samples with initial ratios of $Ru/Sr=0.98-0.88$ was done using 600 atm oxygen at 700–1120 °C. Figure 1 shows x-ray diffraction patterns with intensities of the Bragg peaks shown on a logarithmic scale to better depict the small amounts of impurity phases for $SrRuO_3$ ($x=1$) samples obtained from 700 and 1120 °C. The sample annealed at 700 °C shows a large amount of RuO_2 impurity phase in addition to the main $SrRu_{1-\upsilon}O_3$ phase. The RuO_2 impurity phase is not visible for the sample annealed at 1120 °C. Based on the observation of dissociation of Ru from $SrRuO_3$ at 700–1000 °C in pure oxygen at 1 atm and at high pressure (as well as from energy dispersive

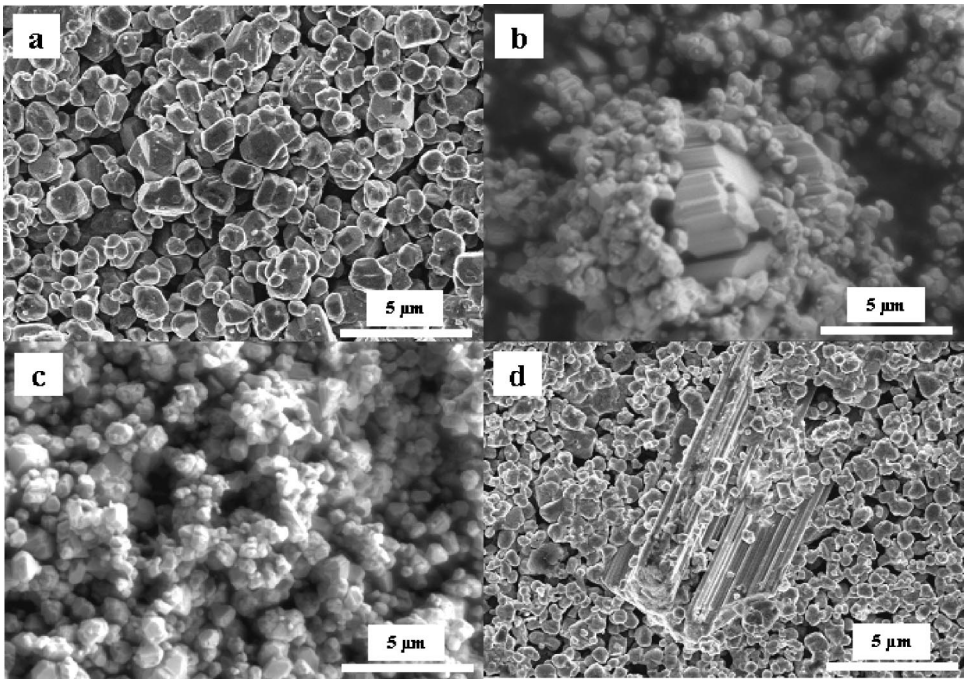

FIG. 2. Scanning electron micrographs of $SrRu_xO_3$ samples. (a) $x=1$, annealed at 1100 °C in air; (b) $x=0.92$, annealed at 1000 °C in air; (c) $x=0.92$, annealed at 1100 °C under 600 atm oxygen pressure; (d) $x=0.88$, annealed at 1100 °C under 600 atm oxygen pressure. (a) and (d) were taken in the secondary electron mode. (b) and (c) were taken in the secondary/backscattered electron mode. Impurity phases are observed in (b) and (d). The beam energy was 5 keV.

x-ray analysis and neutron diffraction measurements that are discussed in following paragraphs) we conclude that both samples annealed at 600 atm O_2 contain large amounts of Ru vacancies for the main $SrRu_{1-v}O_3$ phase. For the sample fired at 1120 °C, the RuO_2 impurity phase is not visible in the diffraction patterns presumably because it volatilized during the long annealing at high temperature and high pressure. High-pressure oxygen annealing of the two-phase samples with $x=0.98-0.92$ at 1120 °C resulted in the formation of single-phase $SrRu_{1-v}O_3$. In analogy to the $x=1$ sample we infer that these samples also contain large amounts of Ru vacancies. A two-phase sample with an initial Ru/Sr ratio of $x=0.88$, after high-pressure oxygen annealing, shows a majority of the $SrRu_{1-v}O_3$ phase and a small amount of unidentified impurity phases.

III. SAMPLE CHARACTERIZATION WITH ELECTRON MICROSCOPY

Sample morphology was studied by SEM (Fig. 2) which shows a quite small average grain size of $0.5-2$ μm. The $x=1$ sample annealed in air [Fig. 2(a)] shows a uniform distribution of similarly shaped irregular grains. An improvement of the crystallinity after the high-pressure oxygen annealing is manifested by an increased number of grains exhibiting clear faceted faces for the $x=0.92$ sample [Fig. 2(b) and 2(c)]. The $x=0.92$ sample synthesized in air [Fig. 2(b)] shows a second phase impurity whose grains are considerably larger ($2-5$ μm) and regular in shape. The same sample after high-pressure oxygen annealing [Fig. 2(c)] does not show impurity phases. The $x=0.88$ sample obtained from high-pressure oxygen annealing shows large-size and regularly shaped grains of an impurity phase [Fig. 2(d)]. All SEM observations performed on single-phase and multiphase samples are in perfect agreement with the results of x-ray diffraction measurements. EDXS compositional analysis was performed on the same samples that were used in SEM studies. By normalizing the Sr content to unity, the average Ru content of the small grains was found to be 0.98(3) and 1.02(5), respectively, for the $x=1$ and $x=0.92$ samples synthesized in air. The average Ru content of the large-grain, second phase impurity observed for the $x=0.92$ sample synthesized in air is close to 0.5, thus, confirming that this phase is Sr_2RuO_4. The Ru content of the small grains was found to be 0.88(4) and 0.85(5) for the high-pressure oxygen annealed samples of $x=0.92$ and 0.88, respectively. The Ru content of the grains of the second phase present for the $x=0.88$ sample after high-pressure oxygen annealing was close to 0.67, indicating that this unidentified phase has a nominal composition $Sr_3Ru_2O_y$. We, thus, conclude that the $x=0.88$ sample has starting composition beyond the solubility limit of Ru-vacancies achievable in 600 atm of O_2. The EDXS quantitative analysis indicates that before the high-pressure annealing, the Ru/Sr ratio is essentially 1.00 for the majority phase independent of the initial stoichiometry x. The measured Ru concentrations for various samples studied with EDXS are displayed in Fig. 4(a) versus the ferromagnetic transition temperature. After annealing, the Ru concentrations are decreasing systematically for samples with larger initial nonstoichiometry of Ru/Sr. This trend of Ru deficiency also agrees with EELS results acquired from areas less than 1 nm in diameter on single crystal grains before and after the annealing.[14]

IV. MAGNETIC AND RESISTIVE PROPERTIES

The temperature dependence of the ac susceptibility in zero-magnetic field is presented in Fig. 3(a) for $SrRuO_3$ samples annealed in Ar at 1100 °C, oxygen at 1100 °C, and high-pressure oxygen at 1120 °C and for an $x=0.92$ sample

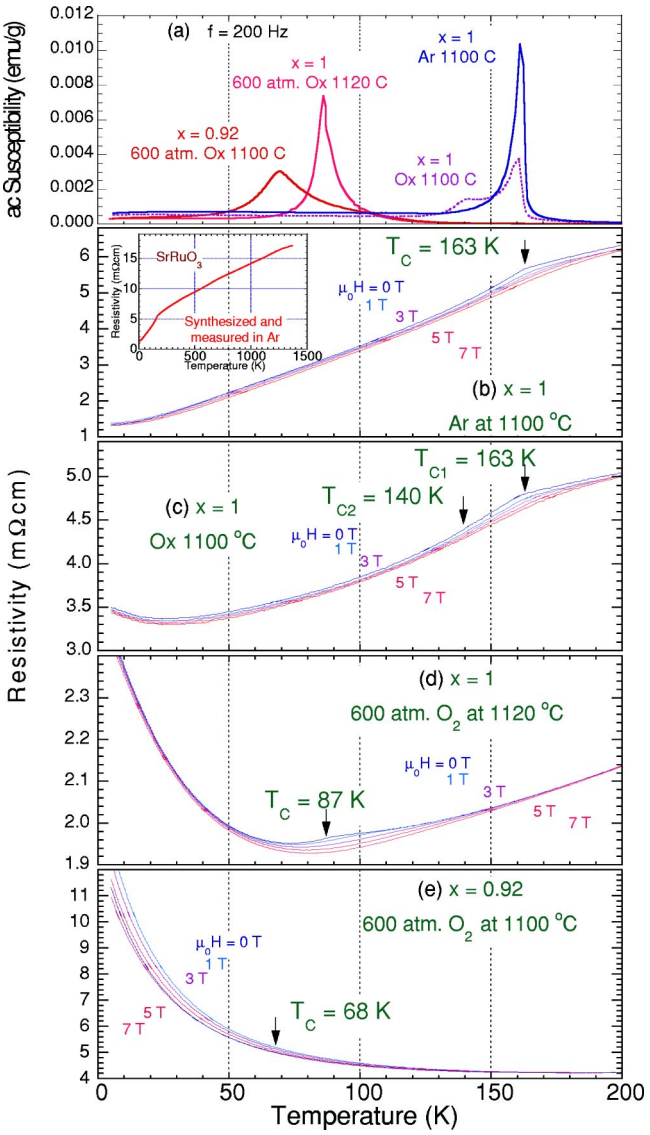

FIG. 3. (Color online) Temperature dependencies of the magnetic ac susceptibility (a) and dc resistivity for samples with starting Ru/Sr ratios (x) that were obtained using the following conditions: (x=1) argon at 1100 °C (b), (x=1) oxygen at 1100 °C (c), (x=1) 600 atm O_2 at 1120 °C (d), and (x=0.92) 600 atm O_2 at 1100 °C (e). Inset to (b) shows resistivity over a wide temperature range for the x=1 sample annealed in argon at 1100 °C.

annealed at high-pressure oxygen at 1120 °C. For the Ar-annealed sample we observe a sharp increase in the ac susceptibility on decreasing temperature at 163 K followed by a slower decrease at lower temperatures. This behavior, in agreement with dc magnetization data (not shown), indicates a uniform ferromagnetic transition that is characteristic of a high quality homogeneous $SrRuO_3$ sample. For the sample obtained from annealing in oxygen, two transitions are seen at 163 K and ~140 K. This result is similar to observations by Joy *et al.* (Ref. 7) for samples synthesized in oxygen at temperatures lower than 1100 °C. For the high-pressure-oxygen annealed $SrRuO_3$ sample, the initial increase in ac susceptibility is not as sharp as for the Ar annealed sample and reaches a maximum at a significantly lower temperature of ~87 K. Finally, the x=0.92 sample annealed at high-pressure oxygen shows the broadest transition at 67 K. The lowest T_C=45 K was observed for the x=0.88 sample that contained small amounts of impurity phases. In general, we have observed that transitions are broader for high-pressure oxygen annealed samples indicating a wider distribution of T_C's. These broader transitions can be interpreted in terms of a slightly inhomogeneous distribution of Ru-vacancies across the grains of material. Such an inhomogeneous distribution of Ru vacancies may also explain the two T_C transitions observed for the oxygen annealed x=1 sample. We define the Curie temperature, T_C, as the temperature of the maximum in the zero-magnetic field ac susceptibility curve.

The temperature dependence of the resistivity in several dc fields is presented in Figs. 3(b)–3(e) for the same set of samples as shown in Fig. 3(a). All samples show metallic behavior near room temperature and the inset to Fig. 3(b) confirms metallic resistivity up to 1373 K (1100 °C) for a sample synthesized in Ar. However, with decreasing temperature, progressively more insulating behavior is seen for samples with decreasing T_C. All samples, with the exception of the samples with the lowest T_C (and the largest amount of Ru-vacancies), show a clear decrease of resistivity below the ferromagnetic transition temperature. When visible, the resistive transition gives values for T_C similar to those obtained from magnetic measurements. All samples show resistivities considerably higher than the resistivities of single crystal samples.[15] The best residual resistivity ratio $R(300\ \mathrm{K})/R(4\ \mathrm{K})$ is observed for the sample made in Ar. However, even for that sample the increased value of resistivity clearly indicates a considerable contribution of grain boundary resistance to the measured values. In addition, we can observe a small negative magnetoresistance present for all samples near T_C and extending to lower temperatures. The magnetoresistance behavior over an extended temperature range indicates a magnetic field dependent scattering at the grain boundaries and a high spin polarization of the electron density at the Fermi energy.[16]

V. NEUTRON POWDER DIFFRACTION

Neutron powder diffraction was used to identify the defects responsible for the decrease in T_C upon annealing in high-pressure oxygen. TGA and EDXS measurements suggested that formation of Ru vacancies was the explanation. Using neutron powder diffraction, it was possible to confirm the existence of these vacancies and establish the relationship between T_C and vacancy concentration in $SrRu_{1-v}O_3$. Neutron diffraction measurements were done on samples that showed the best-defined Curie temperatures. All samples studied by neutron diffraction were single phase with the exception of the x=0.88 sample that showed small unidentified impurity peaks. One would expect that extraction of the Ru atoms from their crystallographic sites to form Ru vacancies would lead to the formation of a Ru-containing secondary phase. However, no such phase was observed in the high-resolution neutron diffraction data indicating that either the RuO_2 impurity phase is not present due to volatilization during annealing (as suggested by the TGA measurements) or

that its grain size is smaller than the coherence length (~100 Å) required for diffraction peaks to be visible. Because electron microscopy did not reveal additional small-size grains of impurity phases for the high-pressure annealed samples we conclude that the RuO_2 impurity phase is not visible because it volatilized during annealing.

In the neutron powder diffraction data, neither superstructure diffraction peaks nor unusual peak broadening were detected for the high-pressure annealed samples. Thus, the room-temperature crystal structures for all samples were refined in the orthorhombic space group *Pbnm* consistent with previous reports.[17] This refinement model immediately led to the conclusion that vacancies were formed on the Ru site and the Sr and O sites were fully occupied within the accuracy of the refinements.

The refined Ru and oxygen site occupancies (with the Sr-site occupancy held fixed at unity) are shown in Figs. 4(a) and 4(b) versus T_C. The data clearly reveal a nominally linear relationship between Ru vacancy concentration and T_C while oxygen content remains unchanged. The maximum concentration of Ru-vacancies introduced by high-pressure annealing was found for the sample with a starting Ru/Sr ratio of $x=0.88$, for which the refinement gave Ru content 0.87(1) ($v \approx 0.13$). The refined site occupancy for nominally stoichiometric sample with $x=1$ and $T_C=163$ K synthesized in air is $\approx 0.96(1)$ ($v \approx 0.04$). This magnitude of Ru-vacancies is larger than the estimated error bar and may indicate the existence of intrinsic Ru-vacancies present for optimally synthesized material. However, considering EDXS and nuclear magnetic resonance measurements[18] indicating stoichiometric and highly ordered samples for this composition obtained in air and Ar as well the TGA measurements described previously, it is likely that this Ru-deficiency is a result of a systematic error in modeling the crystal structure by Rietveld method. The Ru concentrations determined from EDXS measurements are shown for comparison in Fig. 4(a) and, when taken together with the neutron diffraction results, demonstrate Δv clear decrease of T_C from 163 to 45 K with an increase of the amount of Ru-vacancies of ≈ 0.09.

One might expect some substantial variations of structural parameters as a function of Ru vacancy concentration. However, the observed structural changes are rather subtle. The refined lattice parameters at room temperature as a function of T_C display a small, but systematic, dependence on the ferromagnetic transition temperature with larger lattice parameters for lower T_C. Thus, the unit cell volume [Fig. 4(c)] is inversely proportional to T_C. Lattice parameters of $a=5.572$, $b=5.533$, and $c/\sqrt{2}=5.550$ Å for samples synthesized in air and Ar are virtually identical to those reported previously by Jones *et al.* (Ref. 17).

The Ru formal valence would be expected to increase as a result of the reduced amount of Ru in the $SrRu_{1-v}O_3$ compound according to the formula $4/(1-v)$. An increase of the Ru formal valence leads to a smaller ionic size of the Ru ion, and, therefore, to smaller Ru-O interatomic distances because of the partial removal of the *d*-electrons from the antibonding t_g orbitals. This bond-length decrease for the B-site cations in perovskites usually causes a decrease of the lattice parameters and contraction of the unit cell volume. The magnitude of the expected decrease of average interatomic distance ⟨Ru-O⟩ introduced by the change in the formal valence of Ru can be estimated by considering a difference of the Ru ionic sizes between compounds with Ru^{4+} (0.62 Å) and Ru^{5+} (0.565 Å).[19] Using the measured amount of the vacant sites ($\Delta v \approx 0.09$), the change of the Ru formal oxidation state between the sample obtained in air or Ar and the most Ru-deficient material can be estimated from the formula, $4/(1-\Delta v)-4 \approx 0.40$ by assuming that each vacant site remains charge neutral. These large changes of the Ru formal oxidation state should result in a decrease of the average interatomic distance of Δ ⟨Ru-O⟩ ≈ 0.022 Å. The bond-length decrease is, however, not manifested in the refinement results in a straightforward way because the refinements yield the

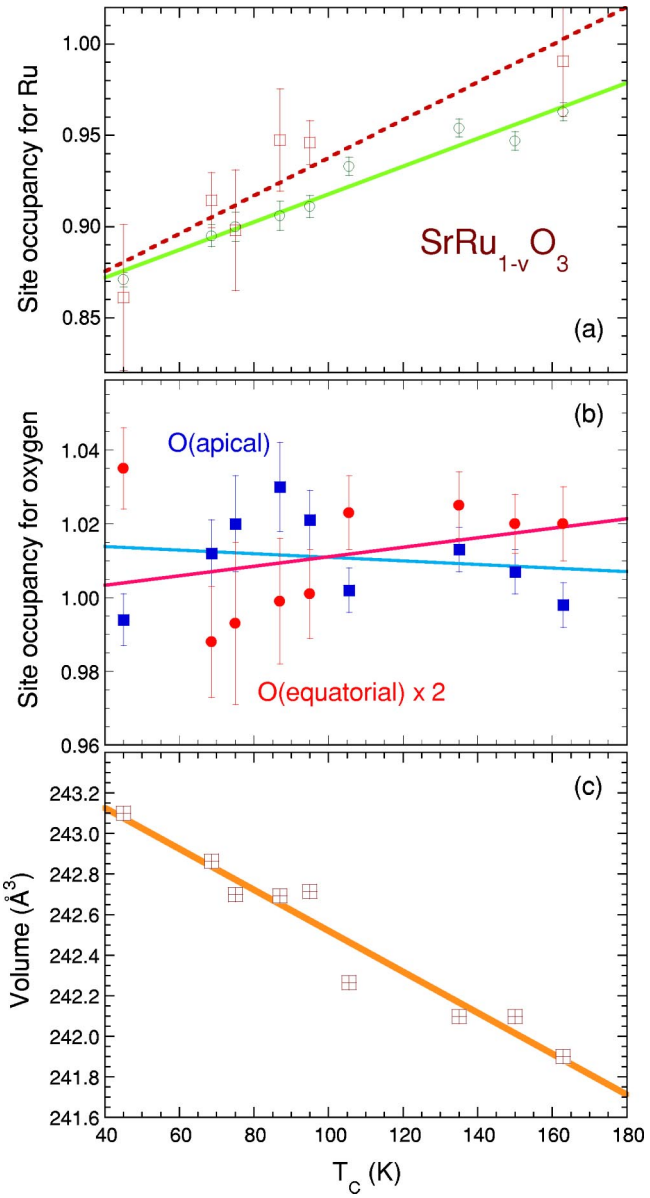

FIG. 4. (Color online) Structural parameters at 300 K versus ferromagnetic transition temperature for $SrRu_{1-v}O_3$ samples: Site occupancies for (a) Ru from neutron diffraction (open circles) and EDXS (open squares) and (b) apical oxygen (filled squares) and equatorial oxygen (filled circles); (c) unit cell volume.

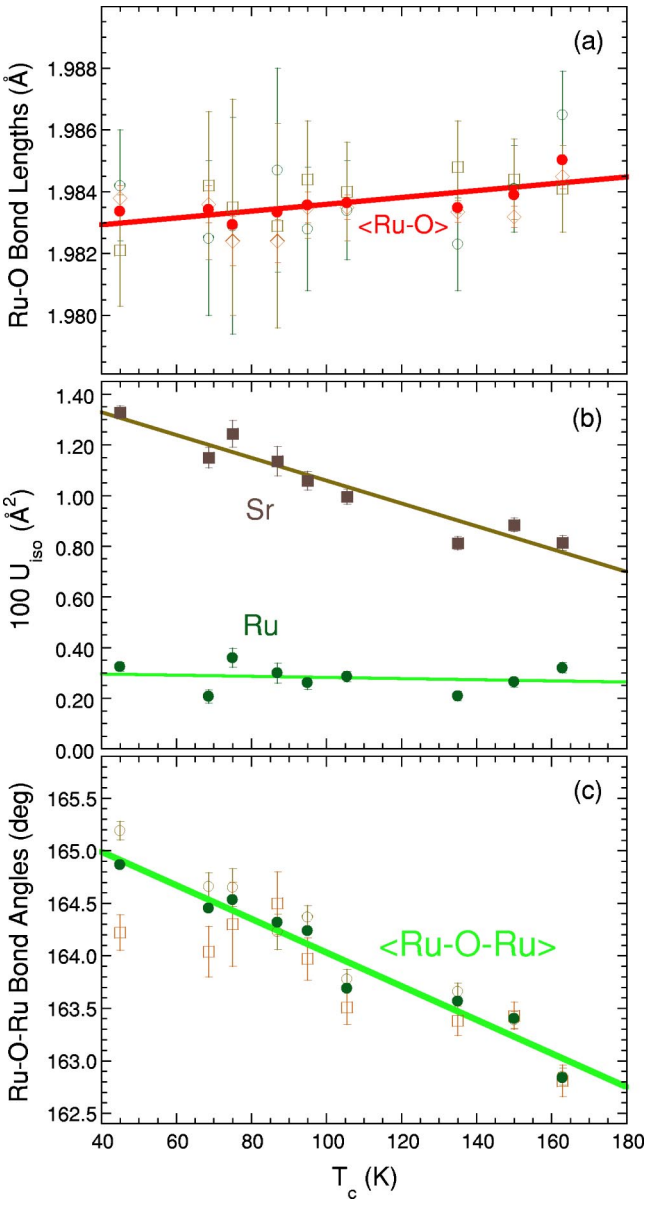

FIG. 5. (Color online) Structural parameters at 300 K versus ferromagnetic transition temperature for $SrRu_{1-v}O_3$ samples: (a) Ru-O bond lengths (open symbols) and average interatomic distance ⟨Ru-O⟩ (filled circles); (b) isotropic thermal parameters for Sr (filled squares) and Ru (filled circles); (c) Ru-O-Ru bond angles (open circles) and their average (filled circles).

average distances from the Ru site (whether occupied or not) to the neighboring oxygen atoms. Figure 5(a) shows this average (Ru-site)-O distance, ⟨Ru-O⟩, versus T_C. Because (Ru vacancy)-O distances are included in the average, the variation is much smaller than would be expected based on change of Ru oxidation state or, for example, bond valence sum calculations. In fact, the nominally constant behavior simply reflects the fact that the average charge state (of Ru atoms plus vacancies) at the Ru site remains constant, i.e., reduced charge screening caused by the Ru-vacancies compensates the expected decrease of the average interatomic distance ⟨Ru-O⟩. As such, the average distance remains very close to the sum of the tabulated ionic sizes of the six-coordinated Ru^{4+} and six coordinated O^{2-} (≈1.984 Å) (Ref. 19). Also, the average refined O-Ru-O bond angles (not shown) remain near 90°. The changes are, thus, different from the typical properties of transition metal perovskites ABO_3, for which an increased formal oxidation state of the B-site cations achieved through oxygen loading or cation deficiency (or substitution) on the A-site leads to decreased B-O interatomic distances, contraction of the unit cell volume, and decreased average structural distortion.

The expected shortening of Ru-O bond lengths resulting from the increase in Ru charge state is manifest, at least qualitatively, in the refined thermal factors *U*. The refined Ru isotropic thermal factor remains essentially constant as Ru vacancies are produced [Fig. 5(b)]. This indicates that the remaining Ru atoms are not displaced from their ideal sites as a result of vacancy formation. In contrast, the thermal factors for both oxygen sites (not shown) increase substantially along the directions of the bonds with the creation of Ru vacancies, consistent with local displacements of oxygen atoms toward occupied Ru sites (which have a higher charge) and away from Ru vacancies.

Perhaps the largest variation in structural parameters is the increase in the isotropic thermal factor of Sr with the creation of Ru vacancies [Fig. 5(b)]. This indicates a rather large static displacement of Sr atoms. A consistent explanation for this is that Sr atoms relax towards vacant near-neighbor Ru sites. In doing so, favorable Sr-O bond lengths can be maintained only if the oxygen-atom sublattice adjusts to accommodate these displacements. This adjustment is observed as a small increase in the average Ru-O-Ru angle [Fig. 5(c)]; i.e., the corner-sharing $RuO_{6/2}$ network unfolds, by rigid rotation of RuO_6 octahedra, to accommodate the Sr displacements. This coordinated unfolding leads to a small positive contribution to the cell volume. Thus, while one might naively expect that the smaller size of Ru ions, resulting from their increased positive charge, would lead to a contraction of the unit cell, just the opposite occurs.

These results clearly show that Ru-site vacancies can be created by processing stoichiometric $SrRuO_3$ samples at high temperature under oxidizing conditions. The use of high-pressure oxygen annealing can extend the vacancy concentration by 9%. The creation of these vacancies dramatically suppresses the ferromagnetic transition temperature—from 163 K for nominally stoichiometric samples to 45 K for a maximum vacancy concentration achievable under high-pressure oxygen conditions of 600 atm. Unusual features of the synthesis and crystal chemistry make the vacancy formation difficult to characterize and have, perhaps, prevented these effects from being understood previously. The RuO_2 formed when Ru is expelled from $SrRu_{1-v}O_3$ is volatile at high temperature and is lost from the sample during processing. Thus, the measured phase fractions of a multiphase sample ($SrRu_{1-v}O_3$ plus RuO_2) cannot be used to prove the existence of Ru-site vacancies or measure their concentration. Additionally, changes in easily measured structural parameters, such as the cell volume, are opposite to what one might anticipate. The expected decrease in Ru-O bond lengths resulting from the increased Ru oxidation state is not directly manifest in the structural data because vacant Ru sites (with lengthened "Ru-O bonds") contribute to the aver-

age ⟨Ru-O⟩ distance. Additionally, as Sr atoms relax towards vacant near-neighbor Ru sites, the average Ru-O-Ru angle increases to maintain favorable local Sr-O bond lengths, giving a positive contribution to the cell volume that offsets the negative contribution expected from decreased Ru-O distances. For these reasons, a direct measurement of the Ru site occupancy, as is provided by the neutron diffraction measurements presented here, is needed to characterize and quantify these defects.

VI. CONCLUSIONS

It future work, it will be useful to fully explore how the thermodynamic conditions of temperature and oxygen partial pressure control the vacancy concentration. This will enable the systematic production of samples with controlled properties. There are also important questions remaining regarding why the ferromagnetic transition temperature is reduced so strongly. A frequently used explanation is that the change in Ru charge state would depress T_C through metallic bandlike effects where the band-filling and the shape of the Fermi surface features are more important than the bandwidth.[1] However, for the reasons previously discussed, it is not possible to estimate the Ru charge state from the diffraction data because the refinements do not yield the local Ru-O distances (i.e., the distances to occupied Ru sites) in the defected structure. Because the change in ferromagnetic transition temperature is so large for a rather small Ru vacancy concentration, one might consider alternative explanations. Clearly, because as shown in Fig. 5(c) the average Ru-O-Ru bond angle increases with decreased T_C; the decrease of T_C is not caused by the weakening of the superexchange interactions arising from a departure of the Ru-O-Ru interaction angle from 180°. Consideration of the magnetic double-exchange mechanism dependence on changing interatomic distance ⟨Ru-O⟩ or bond angle Ru-O-Ru could not explain the decrease of T_C either as the ferromagnetic interactions would be expected to increase on going from stoichiometric $SrRuO_3$ with integer occupancy to charge doped $SrRu_{1-v}O_3$. The data presented here indicate that some other effects, for example, enhanced local disorder that is induced by the Ru defects (Ref. 14) or possibly, more complex effects related to the strongly hybridized $p-d$ orbitals may cause the rapid suppression of T_C for Ru-deficient $SrRu_{1-v}O_3$ samples. Understanding of the sources of different magnetic and electronic properties of the Ru vacancy-doped $SrRuO_3$ from the perovskites of 3*d* transition metals would require accurate first principles studies of the electronic structure near the Fermi energy.

ACKNOWLEDGMENTS

Work at NIU was supported by the NSF-DMR-0105398 and by the U.S. Department of Education. At ANL work was supported by the U.S. Department of Energy, Office of Science under Contract No. W-31-109-ENG-38. We would like to thank Dr. R. E. Cook, Electron Microscopy Center at ANL for valuable assistance. The JEOL 2010F microscope, operated by the RRC at the University of Illinois at Chicago, is supported by the NSF (NSF-DMR-9601792).

[1] I. I. Mazin and D. J. Singh, Phys. Rev. B **56**, 2556 (1997).
[2] G. Cao, S. McCall, M. Shepard, J. E. Crow, and R. P. Guertin, Phys. Rev. B **56**, 321 (1997).
[3] C. B. Eom, R. J. Cava, R. M. Fleming, J. M. Philips, R. B. van Dover, J. H. Marshall, J. W. P. Hsu, J. J. Krajewski, and W. F. Peck, Jr., Science **258**, 1766 (1992).
[4] Z. Fang, N. Nagaosa, K. S. Takahashi, A. Asamitsu, R. Mathieu, T. Ogasawara, H. Yamada, M. Kawasaki, Y. Tokura, and K. Terakura, Science **302**, 92 (2003).
[5] Q. Gan, R. A. Rao, C. B. Eom, J. L. Garrett, and M. Lee, Appl. Phys. Lett. **72**, 978 (1998).
[6] J. J. Neumeier, A. L. Cornelius, and J. S. Schilling, Physica B **198**, 324 (1994).
[7] P. A. Joy, S. K. Date, and P. S. A. Kumar, Phys. Rev. B **56**, 2324 (1997).
[8] M. Shepard, G. Cao, S. McCall, F. Freibert, and J. E. Crow, J. Appl. Phys. **79**, 4821 (1996).
[9] G. Cao, F. Freibert, and J. E. Crow, J. Appl. Phys. **81**, 3884 (1997).
[10] T. He and R. J. Cava, Phys. Rev. B **63**, 172403 (2001).
[11] J. Toepfer and J. B. Goodenough, Chem. Mater. **9**, 1467 (1997).
[12] J. D. Jorgensen, J. J. Faber, J. M. Carpenter, R. K. Crawford, J. R. Haumann, R. L. Hitterman, R. Kleb, G. E. Ostrowski, F. J. Rotella, and T. G. Worton, J. Appl. Crystallogr. **22**, 321 (1989).
[13] A. C. Larson and R. B. von Dreele, *General Structure Analysis System* (University of California, 1985–1990).
[14] Y. Ito, R. E. Cook, P. W. Klamut, B. Dabrowski, and M. Maxwell, Microsc. Microanal., **8, Suppl. 2**, 582CD (2002).
[15] L. Capogna, A. P. Mackenzie, R. S. Perry, S. A. Grigera, L. M. Galvin, P. Raychaudhuri, A. J. Schofield, C. S. Alexander, G. Cao, S. R. Julian, and Y. Maeno, Phys. Rev. Lett. **88**, 076602 (2002).
[16] J. J. Versluijs and J. M. D. Coey, J. Magn. Magn. Mater. **226-230**, 688 (2001).
[17] C. W. Jones, P. D. Battle, P. Lightfoot, and W. T. A. Harrison, Acta Crystallogr., Sect. C: Cryst. Struct. Commun. **C45**, 365 (1989).
[18] Z. H. Han, J. I. Budnick, M. Daniel, W. A. Hines, D. M. Pease, P. W. Klamut, B. Dabrowski, S. M. Mini, M. Maxwell, and C. W. Kimball, Physica C **287**, 256 (2003).
[19] R. D. Shannon, Acta Crystallogr., Sect. A: Cryst. Phys., Diffr., Theor. Gen. Crystallogr. **A32**, 751 (1976).